We are IntechOpen, the world's leading publisher of Open Access books Built by scientists, for scientists

6,900
Open access books available

185,000
International authors and editors

200M
Downloads

Our authors are among the

154
Countries delivered to

TOP 1%
most cited scientists

12.2%
Contributors from top 500 universities

WEB OF SCIENCE™

Selection of our books indexed in the Book Citation Index in Web of Science™ Core Collection (BKCI)

Interested in publishing with us?
Contact book.department@intechopen.com

Numbers displayed above are based on latest data collected.
For more information visit www.intechopen.com

9

Metal Fatigue and Basic Theoretical Models: A Review

S. Bhat and R. Patibandla
School of Mechanical and Building Sciences
Vellore Institute of Technology, Tamil Nadu,
India

1. Introduction

1.1 History of metal fatigue

Preliminary understanding about fatigue failure of metals developed in 19th century during industrial revolution in Europe when heavy duty locomotives, boilers etc. failed under cyclic loads. It was William Albert who in 1837 first published an article on fatigue that established a correlation between cyclic load and durability of the metal. Two years later in 1839, Jean-Victor Poncelet, designer of cast iron axles for mill wheels, officially used the term *fatigue* for the first time in a book on mechanics. In 1842, one of the worst rail disasters of 19th century occurred near Versailles in which a locomotive broke an axle. Examination of broken axle by William John Macquorn Rankine from British railway vehicles showed that it had failed by brittle cracking across its diameter. Some pioneering work followed from August Wöhler during 1860-1870 [1] when he investigated failure mechanism of locomotive axles by applying controlled load cycles. He introduced the concept of rotating-bending fatigue test that subsequently led to the development of stress-rpm (S-N) diagram for estimating fatigue life and endurance or fatigue limit of metal, the fatigue limit representing the stress level below which the component would have infinite or very high fatigue life. In 1886, Johann Bauschinger wrote the first paper on cyclic stress-strain behavior of materials. By the end of 19th century, Gerber and Goodman investigated the influence of mean stress on fatigue parameters and proposed simplified theories for fatigue life. Based on these theories, designers and engineers started to implement fatigue analysis in product development and were able to predict product life better than ever before. At the beginning of the 20th century, J. A. Ewing demonstrated the origin of fatigue failure in microscopic cracks. In 1910, O.H. Baskin defined the shape of a typical S-N curve by using Wöhler's test data and proposed a log-log relationship. L. Bairstow followed by studying cyclic hardening and softening of metals under cyclic loads. Birth of fracture mechanics took place with the work of Alan A. Griffith in 1920 who investigated cracks in brittle glass. This promoted understanding of fatigue since concepts of fracture mechanics are essentially involved in fatigue crack characteristics. However, despite these developments, fatigue and fracture analysis was still not regularly practiced or implemented by the designers.

Importance of the subject was finally realised when serious accidents took place around World War II in 20th century that spurred full fledged research work on the subject.

Requirement of war necessitated fabrication of ships quickly and on a large scale. These ships were coined by US as Liberty Ships. Their frames were welded instead of time consuming riveting. Soon there were incidents of ships cracking in cold waters of Atlantic Ocean. As a matter of fact, some ships virtually broke into several parts due to origination of fatigue cracks by sea waves followed by their rapid propagation in cold environment. Sub-zero temperatures drastically diminished the ductility of welds and parent metals thereby making them brittle. As fracture energy of brittle metals is much less than the ductile ones resulting in reduced critical crack sizes in them, fracture took place at the loads that were otherwise found safe in ambient environment. Similarly Comet Jet Airliners fractured and exploded in mid air. A jetliner flying at an altitude of 10,000 m functions like a pressurized balloon with the wall of its fuselage under high tensile stresses. Since the aircraft structure was not designed against fatigue, cyclic aerodynamic loads resulted in nucleation and propagation of cracks through fuselage of the aircraft resulting in its rupture in flight.

1.1.1 Fatigue failure assessment

Several studies have been undertaken to quantify fatigue failures. A world-wide survey of aircraft accidents was reported in 1981 [2] in which the extent to which metal fatigue was responsible for aircraft failures was assessed. A total of 306 fatal accidents were identified since 1934 with metal fatigue as the related cause. These accidents resulted in 1803 deaths. They covered civil and to a limited extent military aircrafts also. Failure of wings and engines were the most frequent causes of fixed-wing accidents while for helicopters, failures of main and tail rotors were found to be the common causes. About 18 fatal accidents per year were attributed to metal fatigue which was an alarming figure.

Fatigue technology has vastly improved since then with the subject gaining more and more importance. Lot of attention is now-a-days being directed towards fatigue and fracture studies of modern and sophisticated technological machines and structures like high speed aircrafts, nuclear vessels, space shuttles, launch vehicles, ships, submarines, pressure vessels, high speed trains etc. which can be devastating in the event of their fatigue failure.

1.2 Fundamentals of fatigue

Metals when subjected to repeated cyclic load exhibit damage by fatigue. The magnitude of stress in each cycle is not sufficient to cause failure with a single cycle. Large number of cycles are therefore needed for failure by fatigue. Fatigue manifests in the form of initiation or nucleation of a crack followed by its growth till the critical crack size of the parent metal under the operating load is reached leading to rupture. Behaviour of metal under cyclic load differs from that under monotonic load. New cracks can nucleate during cyclic load that does not happen under static monotonic load. Importantly, fatigue crack nucleates and grows at stress levels far below the monotonic tensile strength of the metal. The crack advances continuously by very small amounts, its growth rate decided by the magnitude of load and geometry of the component. Also the nucleated crack may not grow at all or may propagate extremely slowly resulting in high fatigue life of the component if the applied stress is less than the metal fatigue limit. However, maintaining that condition in actual working components with design constraints and discontinuities calls for limited service loads which may be an impediment. Therefore, fatigue cracks in most cases are permissible but with proper knowledge of fracture mechanics about the allowable or critical crack size. On the other hand, only two possibilities exist in cracked structure under monotonic load.

The crack can be either safe or unsafe. The component under cyclic load works satisfactorily for years, albeit with hidden crack growth, but ruptures suddenly without any pre-warning. Such characteristics make cyclic load more dangerous than monotonic load.

1.2.1 Fractograph of fatigue surface

The surface having fractured by fatigue is characterised by two types of markings termed as beachmarks and striations [3]. Both these features indicate the position of the crack tip at some point of time and appear as concentric ridges that expand away from the crack initiation site frequently in a circular or semicircular pattern. Beachmarks (sometimes also called clamshell marks) are of macroscopic dimensions, Fig. 1a, and may be observed with unaided eye. These markings are found in components that experience interrupted crack propagation e.g. a machine that operates only during normal work-shift hours. Each beachmark band represents a period of time over which the crack growth occurs. On the other hand, fatigue striations are microscopic in size, Fig. 1b, and can be viewed with an Electron Microscope. A striation forms a part of beachmark and represents the distance by which the crack advances during the single load cycle. Striation width increases with increasing stress range and vice-versa. Although both beachmarks and striations have similar appearances, they are nevertheless different, both in origin and size. There may be literally thousands of striations within a single beachmark. Presence of beachmarks and striations on a fractured surface confirms fatigue as the cause of failure. At the same time, absence of either or both does not exclude fatigue as the cause of failure.

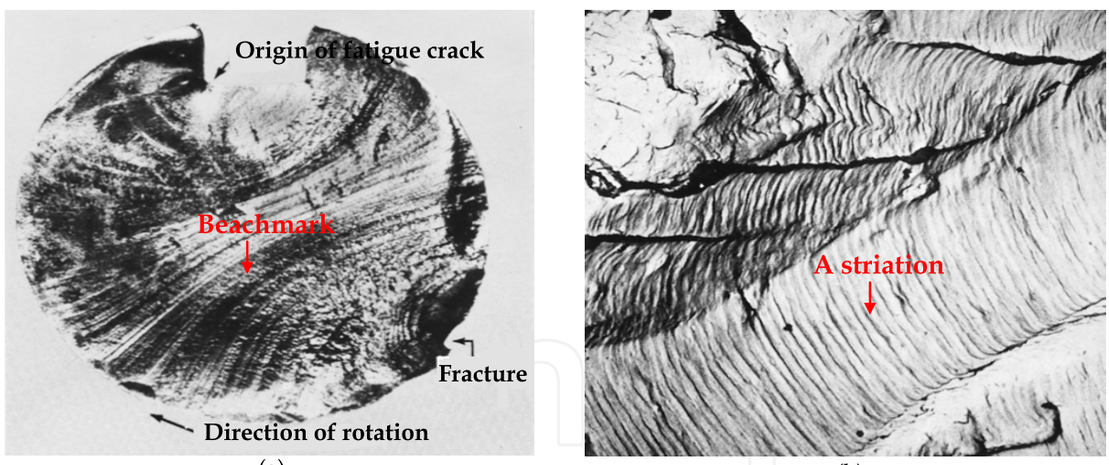

(a) (b)

Fig. 1. Fatigue fracture surface of a steel shaft [3, pp. 216-217]

1.2.2 Types of fatigue load

Load cycles can be of constant amplitude or variable amplitude type. Rotating machines usually operate under pre-decided constant amplitude load cycles whereas aircrafts and ships are subjected to variable amplitude load cycles due to unpredictable and fluctuating wind or sea gusts. Some common types of load cycles are illustrated in Fig. 2. Important fatigue terms are presented.

1.2.3 Classification of fatigue

A. *Load based*: When the stress level is low and the deformation is primarily elastic, the fatigue is called as high cycle type. Number of cycles needed for fracture in this type is high. The account of this regime in terms of stress is more useful. When the stress level is high enough for plastic deformation to occur, the fatigue is known as low cycle type. Number of cycles needed for fracture in such a case is low. The account of this regime in terms of stress is less useful and the strain in the material offers an adequate description. Low cycle fatigue is also termed as strain based fatigue. Direction of load too influences fatigue. Multi-axial loads result in different fatigue characteristics than uni-axial loads. Fatigue under pure mechanical loads is rate independent.

B. *Environment based*: Fatigue characteristics are affected by operating temperature and aqueous and corrosive environments. Fatigue under high temperature is rate dependant.

1.2.4 Factors influencing fatigue life

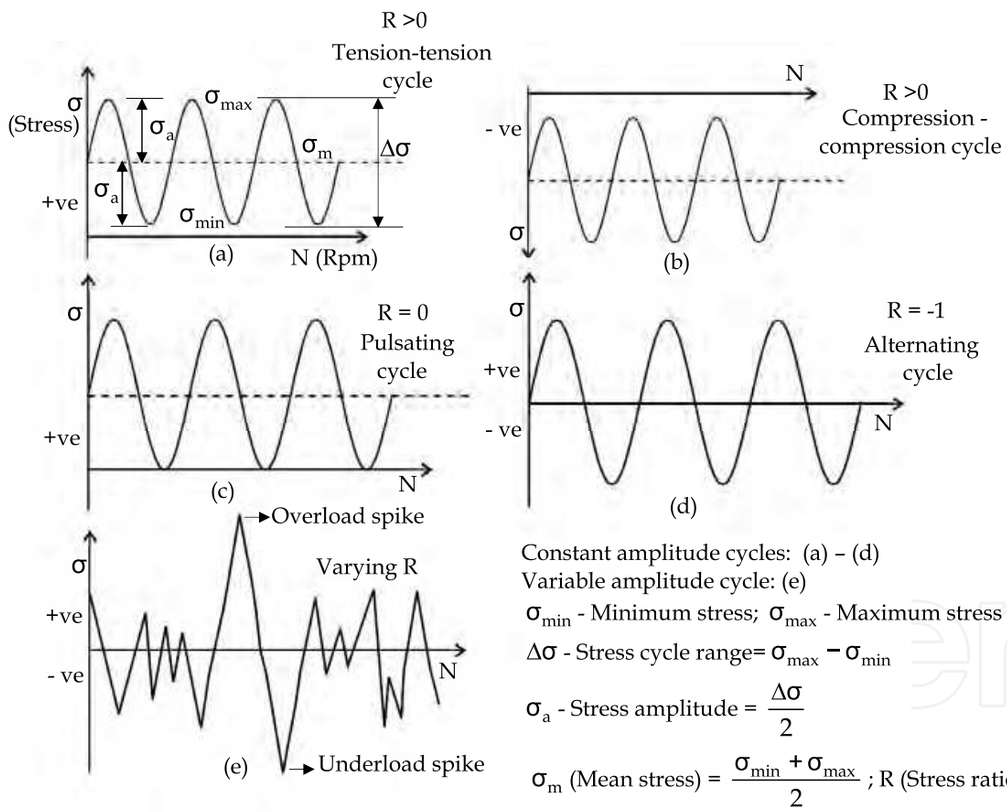

Fig. 2. Types of fatigue cycles

A. *Metal microstructure*: Metal with large grains have low yield strength and reduced fatigue limit and vice-versa. However, at higher temperatures, the coarse grained metal is seen to show better fatigue properties. Barriers to crack growth in the form of precipitates, impurities, grain boundaries, etc. improve fatigue properties. Phase transformations occurring during cyclic loading can also influence the fatigue life.

B. *Manufacturing process*: Fatigue properties are better in the direction of forging, extrusion and rolling and are lower in the transverse direction. Some specific processes like shot peening, cold rolling etc. and other hardening/heat treatment methods that induce compressive residual stresses reduce the chances of crack initiation and enhance the fatigue properties. Tensile residual stresses on the other hand promote crack initiation. Other manufacturing processes like forming, drawing, forging, extrusion, rolling, machining, punching etc., that produce rough surfaces, decrease fatigue life. A rough surface possesses more crack initiation sites due to unevenness and asperities. Polished and ground surfaces on the other hand have excellent high fatigue life due to minimum asperities.

C. *Component geometry*: Discontinuities such as holes, notches and joints, that are the source of stress risers, facilitate crack initiation. Fatigue life of a notched component is less than that of an un-notched one when subjected to similar loads.

D. *Type of environment*: Aqueous and corrosive environments promote crack initiation and increase crack growth rate although crack tip blunting and closure due to accumulation of environmental products at crack tip may dip crack growth rate to some extent. But the overall effect of such environments is to enhance crack growth rate. Under high temperature too, fatigue resistance in most metals generally diminishes with increase in crack growth rate due to the effect of creep.

E. *Loading condition*: Multi-axial loads reduces fatigue life in comparison with uni-axial loads except in the case of pure torsional loading. Mean stress also influences fatigue life. Positive tensile mean stress reduces fatigue life whereas negative mean stress may increase it. The influence of mean stress is more significant in low strain or high cycle fatigue regime.

1.2.5 Fatigue life prediction

1.2.5.1 Constant amplitude load

As discussed earlier in Section 1.1, Wöhler's S-N curves, that were based on experimental fatigue data, were first used for life prediction of metallic structures. A rotating bending test machine is used to obtain S-N curve. The number of cycles, N_f, needed for the specimen to fail when subjected to alternating cycles (R=-1) with maximum stress, σ_{max}, or stress amplitude, σ_a, are recorded. N_f represents fatigue life under σ_{max}. Reduction in σ_{max} enhances N_f and vice versa. Some steels exhibit fatigue or endurance limit whereas non-ferrous metals generally don't. S-N curves have been in use for more than a century now and are still being used by conventional designers. Refer Fig. 3 for S-N curves of various metals. These curves however have certain limitations. They only provide fatigue life without giving any indication about cycles needed for crack initiation and propagation. They also don't take into account the effects of specimen size and geometry i.e. the data generated on a small sized specimen may not be exactly valid for large components in actual use. Also, the component designed on fatigue limit may still fail. S-N curves therefore don't impart sufficient confidence about failure free performance of the component. Consequently, concepts about fatigue damage are required some fatigue damage rules and theories which look into the characteristics of fatigue curves are discussed as follows:

A. *Linear damage rules* (LDR): Refer Fig. 4a and 4b. Basquin in 1910 [4] presented a stress based law, $\sigma_a = \frac{\Delta\sigma}{2} = \sigma_f'(2N_f)^b$, where σ_f' is the fatigue strength coefficient, $2N_f$ is the number of reversals to failure or N_f full cycles and b is the fatigue strength exponent. The stress based approach is mostly applicable in high cycle regime. Coffin and Manson [5, 6] expressed LDR for low cycle regime in terms of plastic strain range as $\frac{\Delta\varepsilon^p}{2} = \varepsilon_f'(2N_f)^c$ where $\frac{\Delta\varepsilon^p}{2}$ is the plastic strain amplitude, ε_f' is the fatigue ductility coefficient and c is the fatigue ductility exponent. For cumulative damage under stress cycles with varying magnitudes, Miner [7] in 1945 first expressed Palmgren's concept [8] in the mathematical form, $D = \sum r_i = \sum \frac{n_i}{N_{fi}}$, where D denotes the quantum of damage, r_i the cycle ratio and n_i and N_{fi} the applied cycles of given stress level and total cycles needed for failure respectively under ith constant amplitude loading cycle. The measure of damage is the cycle ratio with basic assumptions of constant work absorption per cycle. Miner's damage vs cycle ratio plot or D-r curve is a diagonal straight line, that is independent of loading levels. The main deficiencies with LDR are the load level independence, load sequence independence and lack of load-interaction accountability. Life prediction based on linear rule is often un-satisfactory

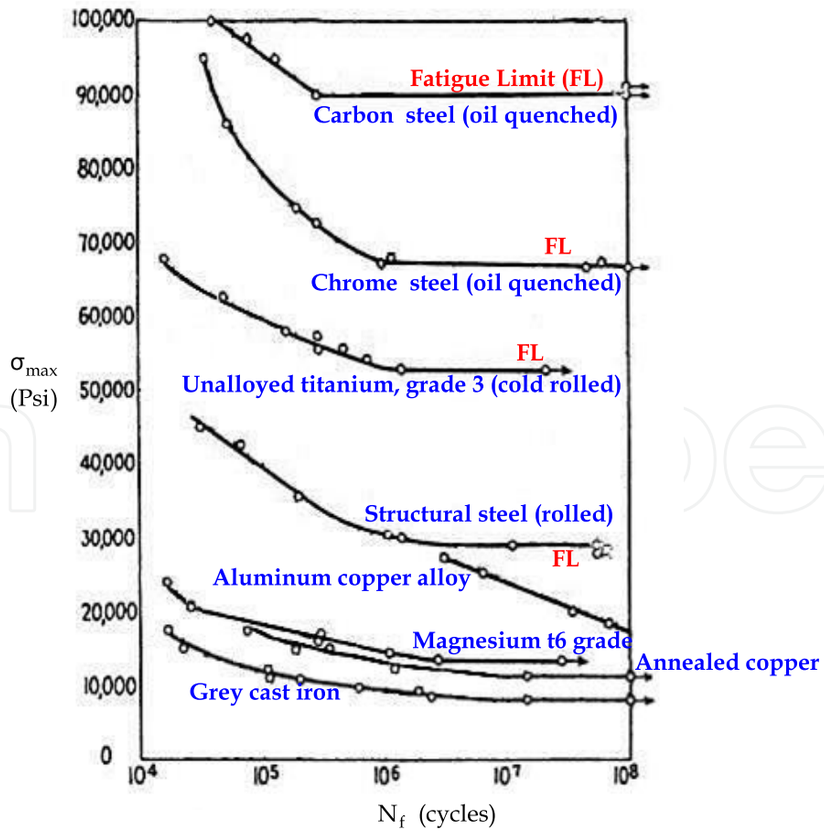

Fig. 3. S-N curves of various metals

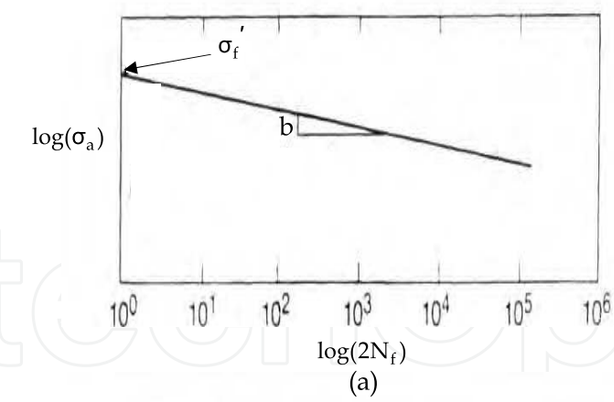

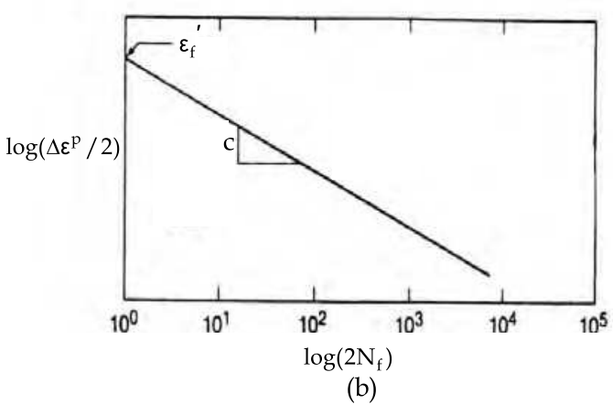

Fig. 4. Stress and strain amplitudes vs number of cycle reversals to failure

B. *Marco-Starkey theory*: Richart and Newmark [9] in 1948 introduced the concept of D-r curves being different at different stress levels. Marco and Starkey [10] followed by proposing the first non-linear load dependant damage theory in 1954 as the power relationship, $D = \sum r_i^{x_i}$, where x_i is a variable quantity related to ith loading. The law results in $\sum r_i > 1$ for low to high load sequence (L-H) and $\sum r_i < 1$ for high to low load sequence (H-L).

C. *Endurance limit reduction theory*: Concept of change in endurance limit due to pre-stress was found to exert an important influence over cumulative fatigue damage. Kommers [11] and Bennett [12] investigated the effect of fatigue pre-stressing on endurance properties using a two-level step loading method. Their experimental results suggested that the reduction in endurance strength could be used as damage measure. Such models are non-linear and are able to account for load sequence effect. But these models fail to include load interaction effects.

D. L*oad interaction effect theory*: Corten-Dolon [13] and Freudenthal-Heller models [14] are based on these theories. Both of them are based on modification of S-N diagram, the results being clockwise rotation of original S-N curve around a reference point on the curve. In the former model, a point corresponding to the highest load point is selected as the reference point while in the latter this reference is chosen as the stress level corresponding to fatigue life of $10^3 - 10^4$ cycles. Fig. 5 shows a schematic of fatigue life for two level L-H and H-L stressing with Corten-Dolon model. Actual values of N_f are indicated.

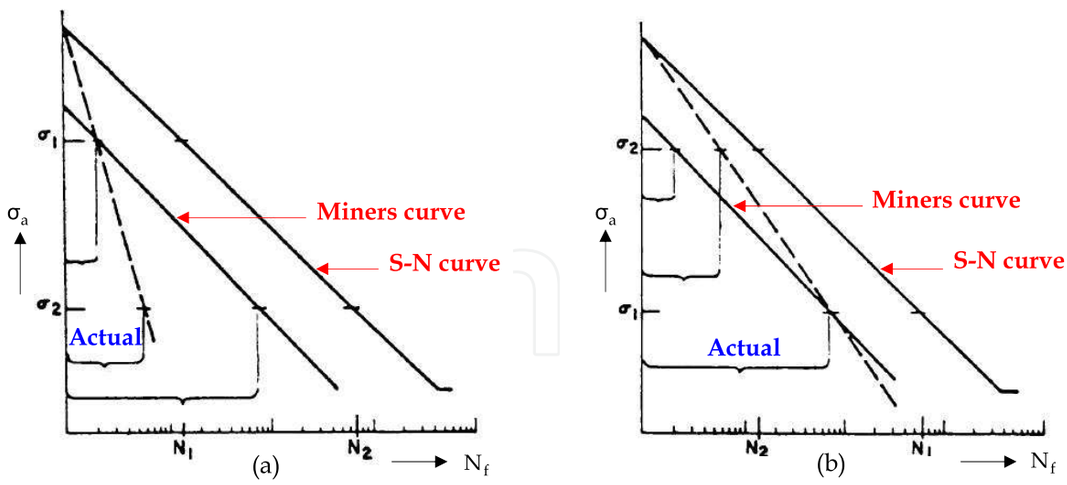

Fig. 5. Fatigue behaviour by rotation method for (a) L-H and (b) H-L load sequences

E. T*wo-stage or double linear damage rule* (DLDR): Using Langers concept [15], Grover [16] considered cycle ratios for two separate stages in fatigue damage process. They are the damage in stage I due to crack initiation, $N_I = \alpha N_f$, and damage in stage II due to crack propagation, $N_{II} = (1-\alpha)N_f$, where α is life fraction factor for the initiation stage. In other model by Manson [17], $N_I = N_f - PN_f^{0.6}$ and $N_{II} = PN_f^{0.6}$ where P is the coefficient of stage II fatigue life.

F. C*rack growth based theory*: Important theories are subsequently elucidated in small crack and large crack sections

1.2.5.2 Variable amplitude and complex loads

In order to assess the safe life of a part operating under variable amplitude load cycles, the following steps are taken:- i) Reduce complex to series of simple cyclic load loading using a technique such as rainflow analysis ii) Create a histogram of cyclic stresses from the rain-flow analysis to form a fatigue damage spectrum iii) For each stress level, calculate the degree of cumulative damage from the S-N curve and iv) Combine the individual contributions using an algorithm such as Miner's rule discussed previously.

1.2.6 Design approaches

The component subjected to cyclic load should ideally be without cracks and its surface should be ground and polished for high fatigue life. The following principles are adopted in the design based on fatigue considerations:

A. *Safe-life design*: The underlying assumption in this approach is that the service load is well known and fixed e.g. parts of rotating machinery, engine valves etc. The maximum stress in the fatigue cycle should preferably be less than the fatigue limit of the metal to ensure high fatigue life. If the metal does not exhibit a definite fatigue limit, then the allowable stress level corresponding to desirable life cycles, say 10^6 or 10^7 is chosen from S-N curve as the limiting/design value. In some cases, as specified by ASME code, the design is based on maximum shear stress theory of failure. Alternating stress intensity which is equal to twice

the maximum shear stress or difference in principal stresses is used as a design factor in conjunction with ASME fatigue curves.

B. *Fail-safe design*: It is employed when service load is of random nature and contains overload or underload spikes e.g. in aircrafts and ships. Since cracks are unavoidable, the fatigue crack is allowed to grow but the structure is designed in such a way that the crack does not become critical. Crack arrestors are implanted at various positions in the structure. In other words, this concept is based on introducing alternative load bearing members such that failure of one could be tolerated by load redistribution to the remaining members. Structures that don't permit multi-piece parts can't be designed with this principle.

C. *Damage tolerance*: Cracks are allowed in this approach as well but stringent periodic inspections are undertaken to check whether the crack size is below the permissible or critical value. Such inspections are regularly carried out in nuclear and aviation industries. A method is available [18] that provides a rational basis for periodic inspection based on crack growth, taking into account variability of various parameters.

1.3 Important fatigue concepts

A. *Crack tip zones*: Region ahead of crack tip undergoes plastic deformation due to high stress concentration induced by the presence of crack. Strains are very high at the crack tip that cause the tip to blunt thereby reducing the local stress tri-axiality. Refer Fig. 6. The region in immediate vicinity of the crack tip of size, δ^*, in immediate vicinity of the crack tip is called as the process zone. The fracture process resulting in crack advancement by breaking of atomic bonds in the case of brittle metal and coalescence of voids in the case of ductile metal takes place in this zone. The process zone is governed by large strain analysis and Hutchinson, Rice and Rosengren (HRR) elastic–plastic and other stress solutions, that are based upon small strain or deformation plasticity concepts without considering the effect of blunting, are therefore not valid in it. Area ahead of process zone is divided into three regions: Region I or the cyclic plastic zone of size, Δr, where plastic deformation takes place during loading and unloading half-cycles. Region II, between the monotonic plastic zone of size, r_m, and the cyclic plastic zone, where plastic deformation occurs only during the loading part of the cycle and metal is elastic during the unloading part. Region III or the elastic zone beyond the monotonic plastic zone where cyclic strains are fully elastic both during loading and unloading parts of the cycle.

B. *Crack closure*: Refer Fig. 7. During unloading part of a load cycle, the opened crack faces touch each other earlier at position A instead of B. On further reduction of stress from A, the touched surfaces start exerting compressive load, the effect of which is overcome by a part of the next cycle. In other words, the part of energy of new cycle is utilized in overcoming the compressive effects induced by the previous cycle. In the process, the applied cyclic stress intensity parameter, ΔK, reduces to effective stress intensity parameter, ΔK_{eff}, that is equal to $K_{max} - K_{cl}$. The closure ratio, U, is defined as $U = \frac{\Delta K_{eff}}{\Delta K}$. Closure is induced by factors like crack tip plasticity, surface oxides, surface roughness and operating viscous fluids (if any) and is desirable since it retards crack growth rate.

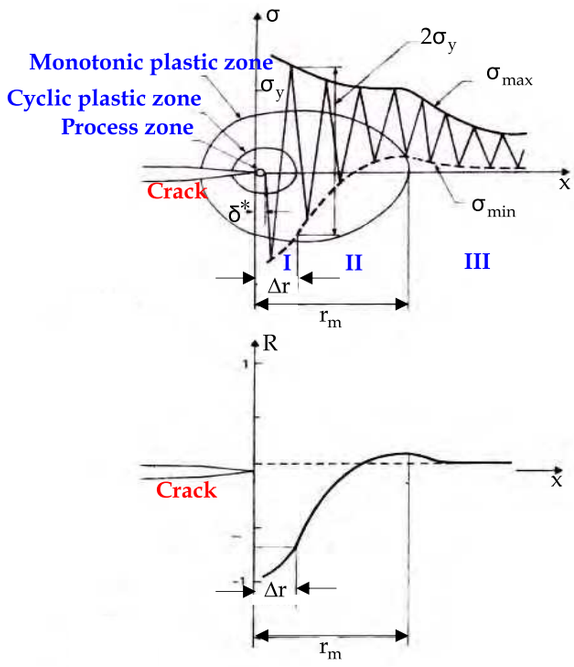

Fig. 6. Fatigue crack tip zones

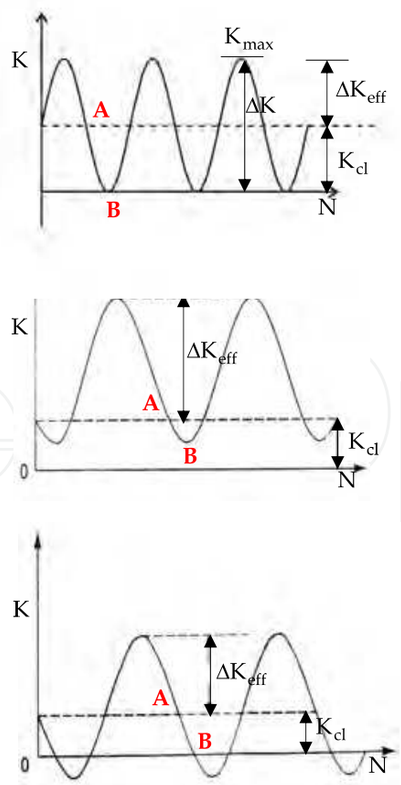

Fig. 7. Crack closure

C. *Threshold*: The condition at which the crack is just able to propagate forward by an infinitesimally small distance before it is arrested again is called the threshold state. The arrest may be due to crack tip blunting or dislocation re-arrangement. Threshold stress intensity parameter is denoted by ΔK_{th} . Experimental threshold measurement is expensive and time consuming. However, there are some empirical models to obtain ΔK_{th} which are based upon the principles of energy and dislocation dynamics. These models consider crack growth by slip at crack tip and assume grain boundaries as principal barriers to slip. Threshold prediction according to energy criterion [19] is of the form $\Delta K_{th} = \sigma_{yc}\left(\frac{2.82\pi d}{1-\nu^2}\right)^{1/2}$ where σ_{yc} is the cyclic yield strength of the metal that is equal to $2\sigma_y$, σ_y being the monotonic yield strength, d the grain size and ν the poisson's ratio of the metal. The energy model, while ignoring micro-structural effects, considers energy as controlling parameter in deciding the physical extent of the plastic zone or crack advance. Dislocation models on the other hand consider behavior of dislocations at the crack tip. Dislocations during slip pile up at the first grain boundary and limit the outward flow of further dislocations from the crack tip. A typical Hall-Petch model suggests, $\Delta K_{th} = A + B\sqrt{d}$, where A and B are material constants. The model also reduces to the concept of a slip band extending from the crack tip to a grain boundary when loaded by stress equal to σ_{yc} . With the help of linear elastic fracture mechanics (LEFM) equation and assuming the slip band to be the crack which will just be able to propagate at the threshold, a following simple relation is written [19, p. 16] as $\Delta K_{th} = \sigma_{yc}\sqrt{\pi d}$. Although this relation is somewhat invalid because of the use of principles of LEFM in plastic stress field, yet it effectively predicts the dependence of grain size and yield strength of metals on their fatigue threshold.

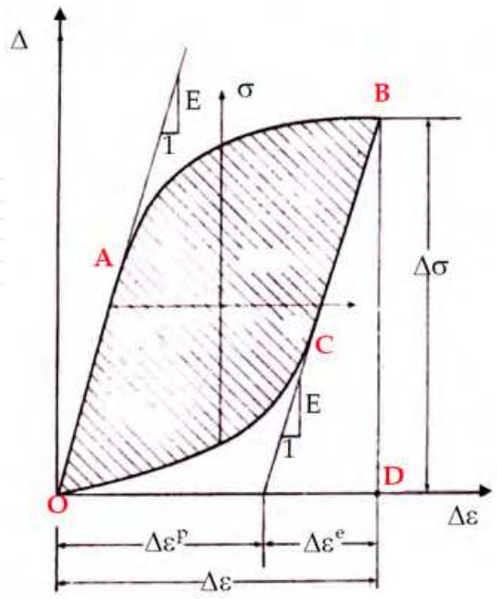

Fig. 8. Hysteresis loop for a masing material

D. *Hysteresis energy*: During cyclic loading, applied energy is dissipated in the form of plastic deformation/slip at the crack tip. Refer Fig. 8. The plastic strain energy or hysteresis energy, ΔW^p, absorbed in a load cycle per unit volume is the area of hysteresis loop (Area OABCO) and for a Masing material it is given as, $\Delta W^p = \frac{1-n'}{1+n'}\Delta\sigma\Delta\varepsilon^p$ [20], where n′ is the cyclic strain-hardening exponent that is equal to zero for an elastic-perfectly plastic material. Method to obtain ΔW^p for a Non-Masing material is explained at [21]. A part of hysteresis energy is consumed in heat and vibration and the remaining part causes damage in the form of crack growth by slip.

2. Fatigue mechanisms

Nucleation and propagation of cracks constitute major fatigue mechanisms. Initiation of fatigue crack at smooth polished surface under ambient conditions may consume nearly 90% of applied cycles while crack propagation may require only remaining 10% cycles. Distribution of cycles changes in defective specimens with environment also playing a major role. The mechanisms and models for crack initiation and growth in specimens without and with the defects in ambient environment are as follows:

2.1 Specimen without notch or defect

2.1.1 Crack initiation

Initiation of a new crack in smooth polished metals under cyclic load is caused by irreversible dislocation movement leading to intrusions and extrusions. (A dislocation is the flaw in the lattice of the metal which causes slip to occur along favorable oriented crystallographic planes upon application of stress to the lattice). These dislocations agglomerate into bundles almost perpendicular to the active Burger's vector. (Burger's vector represents magnitude and direction of slip). Strain localization occurs when dislocation pattern in a few veins or bundles becomes locally unstable at a critical stress or strain thereby leading to formation of thin lamellae of persistent slip bands or PSB's. The subsequent deformation is mainly concentrated in these slip bands as they increase and fill the entire volume of the crystal. If the PSB's are removed by electro-polishing, it will be found by retesting that they reform in the same area and become persistent. That is why the slip bands are also referred to as the persistent slip bands. They are very soft as compared to hard parent metal. Mechanism of formation of PSB's is different in different metals. For example, in a single FCC crystal of copper, the strain in the matrix is accommodated by quasi-reversible to and fro bowing of screw dislocations in channels between the veins. In softer materials which experience large strains, the edge dislocations bow out of the walls and traverse the channels. In poly-crystals, the PSB's are generally found on the grains which have suitable orientations for the slip to occur. Fig. 9 shows a schematic of slip during monotonic and cyclic load. Under monotonic load, slip lines are formed in metal that are sharp and straight and are distributed evenly over each grain. Under high magnification, the individual lines appear as bands of parallel lines of various heights. On the other hand, the slip lines produced under cyclic load form in bands that do not necessarily extend right

across a grain. New slip lines form beside old ones as the test proceeds. Although these bands grow wider and become more dense, there are areas between the bands where no slip takes place. Inhomogenity at the microscopic level, when the plastic strain in the PSB lamellae is at least an order of magnitude higher than the metal matrix, causes the crack to eventually form at the interface of PSB and the matrix. Also across the PSB-matrix interface, there is high strain gradient due to PSB's being softer in nature and the matrix being harder. The deformation compatibility requirement at the interface results in high shear stress along the interface leading to cracks. Crack initiation is aided by environmental effects also. Atmospheric oxygen diffuses into slip bands of PSB's thereby weakening them and accelerating initiation. On the other hand, crack initiation in an inert environment may be retarded by up to two orders of magnitude. Favorable crack initiation sites at micro-level can be stated as:- i) Slip steps between emerging extrusions of PSB's and the matrix ii) At micro notches near outer edges iii) At intrusion sites and iv) Grain boundaries in the case of high temperature and corrosive environment. Cracks once initiated can be viewed, Fig. 10, as per the following categories depending upon their location on the surface grain:- i) Trans-granular, ii) Inter-granular, iii) and iv) Surface inclusion or pore, v) Grain boundary voids and vi) Triple point grain boundary intersections. The last two are found at elevated temperatures. Models to estimate the number of cycles, N_i , for crack initiation are difficult to develop and initiation life is measured experimentally.

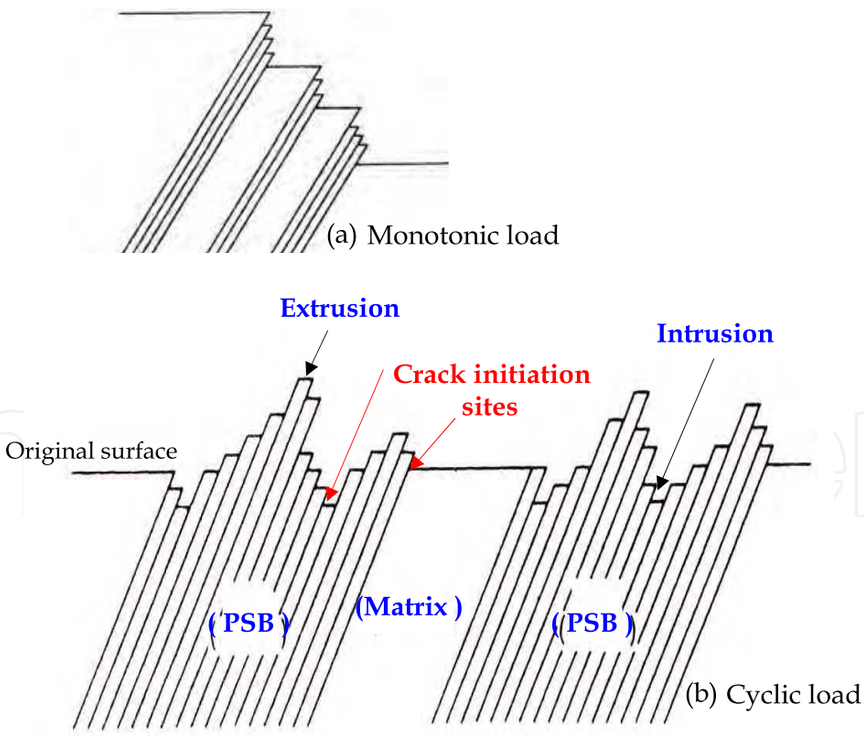

Fig. 9. Schematic of slip under (a) monotonic load and (b) cyclic load [21, p. 13]

New crack initiates from the surface. Firstly, because the surface grains are in intimate contact with the atmosphere, thus if environment is a factor in the fatigue damage process,

the surface grains are more susceptible. Secondly, a surface grain is not wholly supported by adjoining grains. It can deform plastically more easily than a grain inside the body surrounded on all sides by grains. Experiments have been conducted to prove this point. If the surface of the component is hardened, either metallurgically or by surface hardening, the fatigue strength of the specimen increases as a whole. Similarly, any procedure that softens the surface decreases the fatigue strength. It has been shown that if a fatigue test is stopped after some fraction of the expected specimen life, with thin layer of metal removed from the surface of test specimen and the test restarted at same stress level, the total life of the specimen goes up. Since large number of fatigue cycles is consumed in crack initiation, removal of surface layer at frequent intervals enhances the fatigue life manifold.

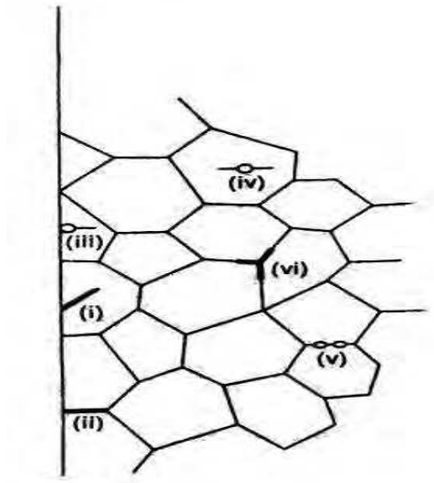

Fig. 10. Crack initiation sites [21, p. 16]

2.1.2 Crack growth

Since growth mechanism and propagation rate of a crack differs according to its size, it is essential to define the crack based on its size in increasing order, Refer Fig. 11 :- i) Metallurgically or micro-structurally small crack which is small as compared to a metallurgical variable such as the grain size. Such a crack is strongly affected by microstructure of the metal and its growth stops at micro-structural barriers if the applied stress level is below the fatigue limit of the metal. The size of this crack would generally be of the order of 1 grain. Refer Fig. 12 and Fig. 13. Its growth rate decreases with increasing length ii) Physically small crack in which the resistance to crack growth by micro-structural barriers is averaged out but it is not long enough to be called a long crack. Length of physically small crack is of the order of 3 to 4 grain size. Such a crack is also arrested at micro-structural barriers if the stress level is below the fatigue limit but it has different characteristics in comparison with long crack. It grows at threshold value of ΔK below that of a long crack and propagates at higher rate than a long crack for same value of ΔK . Like micro-structurally small crack, its growth rate also decreases with increasing length in each successive grain. Knowledge of metallurgically and physically small cracks is necessary from practical point of view as it indicates the size of the flaw or a crack which can be tolerated in the production process. Since crack closure levels are not stable in small cracks,

they can not be dealt with the principles of continuum mechanics iii) Long crack that has stable closure and can be treated by continuum mechanics.

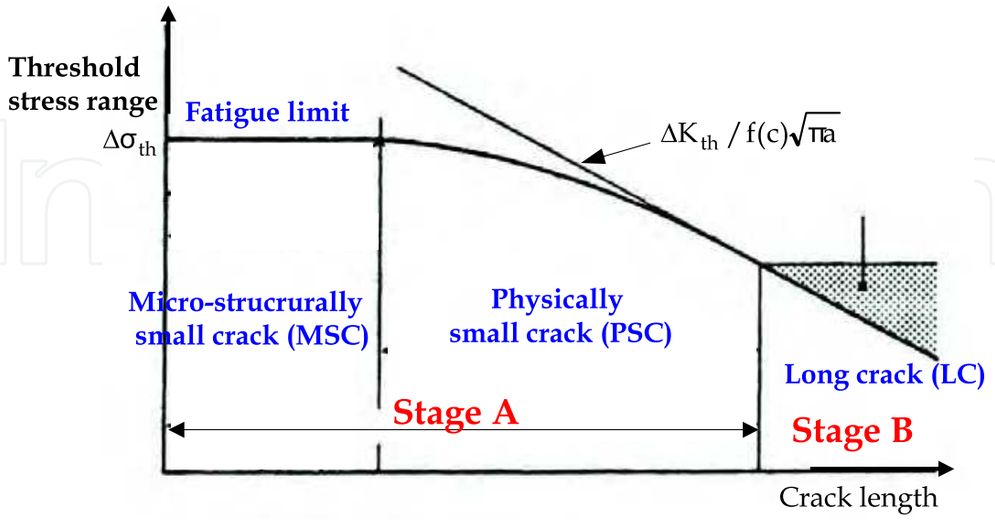

Fig. 11. Three regimes of crack size [21, p. 419]

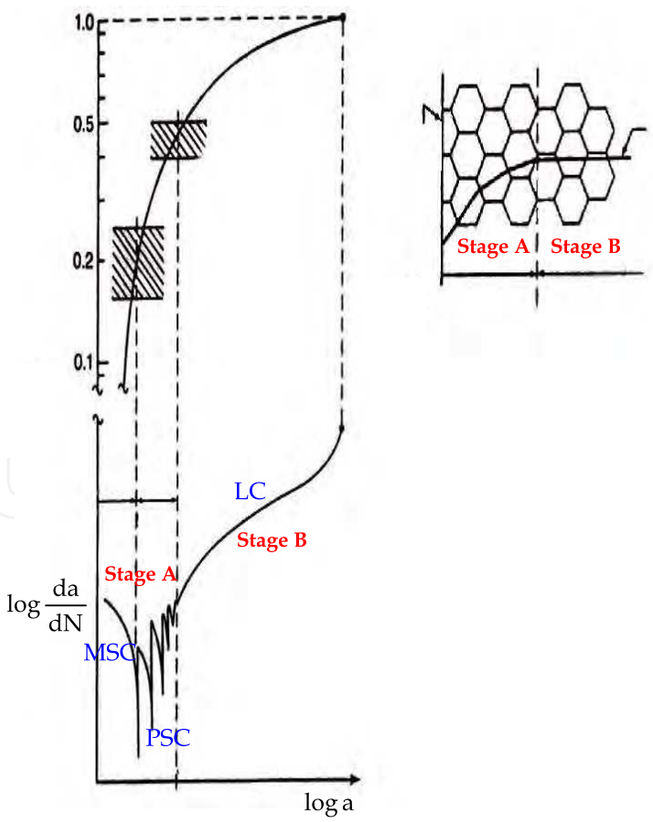

Fig. 12. Transition from small crack to long crack [21, p. 418]

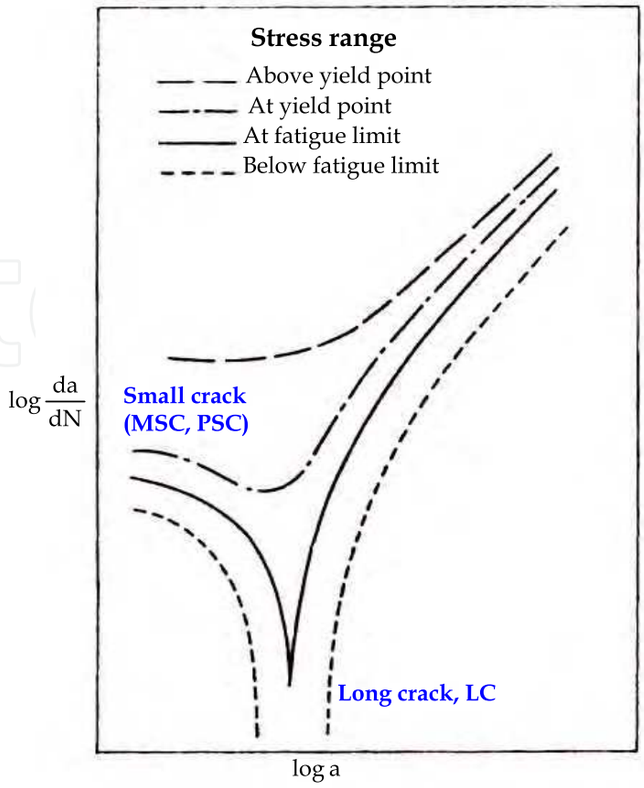

Fig. 13. Crack behavior vs applied cyclic stress [21, p. 416]

2.1.2.1 Small crack growth

The ratio of plastic zone to the overall size of a small crack is much larger than the long crack under same value of applied ΔK. Small crack is therefore strongly influenced by crack tip plasticity. It grows by irreversible plastic deformation at the tip in a slip plane along the slip direction. As shown in Fig. 14a and 14b, an intrusion forms due to the relative displacement of a slip band cc' and the one above it due to shear stress reversal. In the next applied cycle, Fig. 14c, dislocations on cc' plane produce a greater offset. An opposite deformation, Fig. 14d, causes the slip planes above and below cc' to act resulting in the intrusion to eventually grow and form a crack of the order of few micro meters Crack growth is in. small integral multiples of Burger's vector. The magnitude of local cyclic plastic strain ahead of crack tip is a measure of driving force. As the crack approaches a micro-structural barrier, the primary slip becomes incompatible with adjacent grains and the micro-structural induced crack tip shielding decelerates crack growth. As a result, primary plastic zone also decreases resulting in plasticity redistribution. In the process, secondary slip system forms and the crack deviates from the original path leading to crack branching. The secondary slip system plays an important role in increasing crack opening and driving the crack across the micro-structural boundary. Once the path of the crack is altered, the roughness induced closure by mixed sliding and mismatch between crack face asperities again dips the crack driving force and growth rate. The models describing threshold and small crack behaviour are essentially micro-structure based and are as follows [4]:

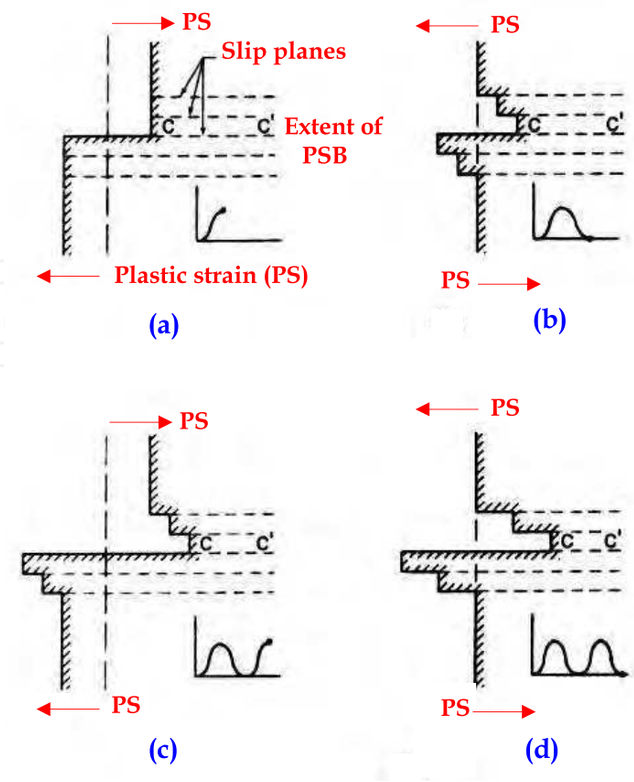

Fig. 14. Stages of small crack growth [21, p. 421]

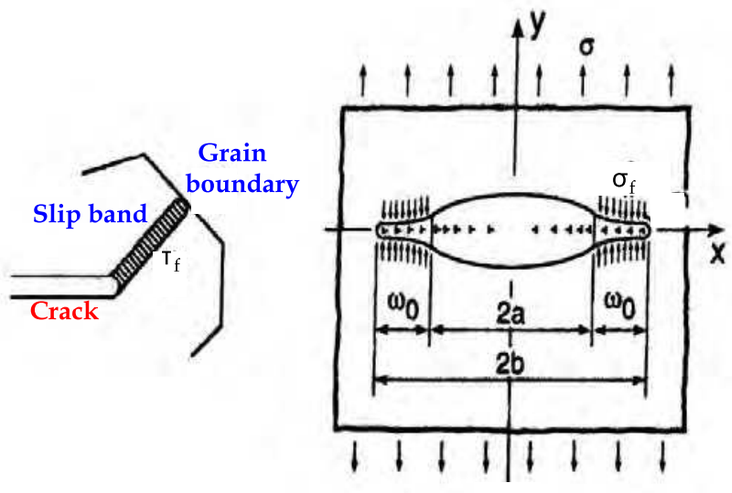

Fig. 15. Schematic of slip band model [21, p. 430]

A. Threshold models [21, pp. 430-435]

A.1 *Slip based model*: The threshold stress for short crack is defined in terms of slip band grain boundary interactions. In this model, the required condition for co-planar slip bands emanating from the crack tip when blocked by grain boundary is investigated. Fig. 15 shows a schematic of this model. An analysis of this condition yields:

$$\Delta\sigma_{th} = \frac{\Delta K_{th}}{\sqrt{\pi a}} = \frac{\Delta K_m}{\sqrt{\pi b}} + \frac{2}{\pi}\Delta\sigma_f \arccos\left\{\frac{a}{b}\right\} \quad (1)$$

where $\Delta\sigma_{th}$ is the threshold stress range, $\Delta\sigma_f$ is the frictional stress range for dislocation motion, ΔK_m is the microscopic stress intensity parameter range at the tip of slip band, 2a is the crack length, $b = a + \varpi_o$ where ϖ_o is the width of blocked slip band. The fatigue limit is obtained from above, by letting a = 0 i.e. a very small crack, in Eq. (1) as

$$\Delta\sigma_e = \frac{\Delta K_m}{\sqrt{\pi\varpi_o}} + \Delta\sigma_f \quad (2)$$

A.2 *Surface strain redistribution type model*: The model is based on non-uniformity of strains in surface layer and the development of crack closure. The surface grains oriented for easy slip are subjected to an inherent micro-structurally dependant strain concentration which decays with the depth into the material. The threshold stress range is defined as

$$\Delta\sigma_{th} = \frac{\Delta K_{th} U_{cl}}{FQ\sqrt{\pi a}} \quad (3)$$

where U_{cl} is the crack closure development parameter, F is the shape factor with a value of 0.72 for semicircular surface crack and Q is the stress concentration factor.

B. Crack growth rate model

The model is based on the principle of surface layer yield stress redistribution. In contrast to the previous model at A.2, this model is concerned with the distribution of yield stress through the surface layer. There is ample experimental evidence about the fact that the surface layer is much softer than the bulk material and the yield stress can be significantly lower in surface grains than in the bulk material. The material thickness is subdivided into a series of strips whose thickness is equal to process zone, δ^*. Refer Fig. 16. Total plastic energy density at the m-th layer is the sum of hysteresis energy per cycle and the applied energy at that layer. Hysteresis energy is provided in Section 1.3D. Applied energy given by HRR is of the form , $\Delta\sigma\Delta\varepsilon^p = \frac{\Delta K^2}{Er\psi(n',\theta)}$. On the crack plane, $\theta = 0$, distance of m-th layer from the crack tip, $r = \delta^* + \rho_c$ where ρ_c is critical blunting radius, $\psi(n',\theta)$ depends upon the strength of singularity field and E is the modulus of elasticity of the metal. Taking ρ_c = 0 for a small crack , the expression for total energy at m-th layer near the surface is obtained as

$$(\Delta\sigma\Delta\varepsilon^p)_{m,total} = \left(\frac{1-n'}{1+n'}\right)\Delta\sigma_{ym}\Delta\varepsilon_m{}^p + \frac{\Delta K^2}{E\delta^*\psi(n')} = \left(\frac{1-n'}{1+n'}\right)\Delta\sigma_{ym}\left[\Delta\varepsilon_b - \frac{\Delta\sigma_{ym}}{E}\right] + \frac{\Delta K^2}{E\delta^*\psi(n')} \quad (4)$$

Basquin and Coffin-Manson relationships when coupled give the following

$$(\Delta\sigma\Delta\varepsilon^{p})_{m,total} = 4\sigma_f'\varepsilon_f'(2N_f)^{b+c} \tag{5}$$

Number of cycles, N^*, required for the crack to advance through the process zone, δ^*, at m-th layer is equal to

$$N^* = \frac{1}{2}\left[\frac{(\Delta\sigma\Delta\varepsilon^{p})_{m,total}}{4\sigma_f'\varepsilon_f'}\right]^{\frac{1}{b+c}} \tag{6}$$

On using Eq. (4) and considering crack growth rate per cycle, $\frac{da}{dN}$, as $\frac{\delta^*}{N^*}$, the expression for $\frac{da}{dN}$ is obtained as:

$$\frac{da}{dN} = 2\delta^*\left[\frac{\left(\frac{1-n'}{1+n'}\right)\Delta\sigma_{ym}(\Delta\varepsilon_b - \frac{\Delta\sigma_{ym}}{E}) + \frac{\Delta K^2}{E\delta^*\psi(n')}}{4\sigma_f'\varepsilon_f'}\right]^{\frac{1}{b+c}} \tag{7}$$

Eq. (7) re-confirms that $\frac{da}{dN}$ depends upon soft surface layer properties, crack tip stress-strain range and bulk mechanical and fatigue properties of the metal.

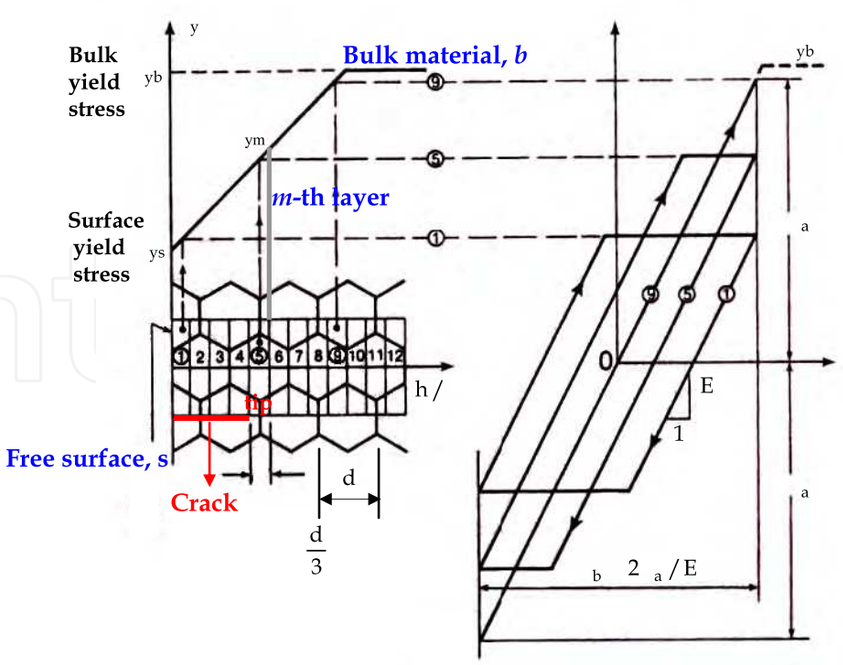

Fig. 16. Material modeling of soft surface layer and three cyclic stress-strain loops near the free surface region in short crack growth [21, p. 434]

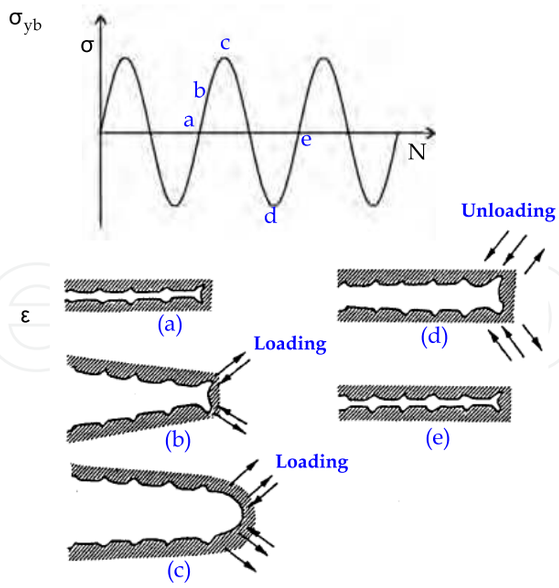

Fig. 17. Plastic blunting model for long crack growth, stages (a) to (e)

2.1.2.2 Long crack growth

Two different mechanisms namely plastic sliding and damage accumulation at the crack tip describe long crack growth in high cycle and low cycle regimes respectively. The plastic sliding mechanism in high cycle regime, proposed by Laird and Smith [22] is also known as the plastic blunting model. Fig. 17 is a schematic of crack tip opening, blunting and crack advance in this model. It can be seen that by application of tensile load, highly localized plastic deformation takes place along the slip planes of maximum shear stress. Upon further increase of load, the width of slip band increases and the crack tip blunts to semi-circular shape. As a result of blunting, the crack extends to about half the crack tip opening displacement. During compressive loading, the direction of slip is reversed and the vertical distance between crack surfaces decreases. The new surface created during tensile load is partly folded by buckling into double notch at the tip. At the maximum compressive stress, the crack tip is sharp again that facilitates further crack growth. In low cycle regime, mechanism for crack growth is based on damage accumulation in the process zone. The crack advances through the zone when sufficient amount of damage is accumulated. The models describing threshold and long crack growth characteristics are as follows:

A. Threshold model: Refer Eq. (1). Threshold condition for long crack where $a >> \varpi_o$ is

$$\Delta\sigma_{th} = \frac{\Delta K_{th}}{\sqrt{\pi a}} = \frac{\Delta K_m}{\sqrt{\pi a}} + \frac{2}{\pi}\left(\frac{2}{a}\right)^{1/2} \Delta\sigma_f \sqrt{\varpi_o} \tag{8}$$

and

$$\Delta K_{th} = \Delta K_m + 2\left(\frac{2}{\pi}\right)^{1/2} \Delta\sigma_f \sqrt{\varpi_o} \tag{9}$$

Special case is obtained by setting $\Delta K_m = 0$ and $\Delta\sigma_f = 2\sigma_y$ in Eq. (1) as follows

$$\Delta\sigma_{th} = \frac{4}{\pi}\sigma_y \arccos\left\{\frac{a}{a+\varpi_o}\right\} \tag{10}$$

Solving for ϖ_o, one obtains

$$\varpi_o = a\left[\sec\left\{\frac{\pi\Delta\sigma_{th}}{4\sigma_y}\right\} - 1\right] \tag{11}$$

which represents Dugdale's plastic or cohesive zone size.

B. Crack growth rate models: The models in different regimes are as follows:

B.1 *High cycle regime*: Refer Fig. 18. The crack growth rate model in region B due to sliding off mechanism is of the form

$$\frac{da}{dN} \approx CTOD = \frac{\Delta K^2}{2E\sigma_y} \tag{12}$$

where CTOD is the crack tip opening displacement. Paris [23] proposed a law

$$\frac{da}{dN} = C(\Delta K)^m \tag{13}$$

where C and m are material properties. In presence of closure, the above law is modified to the form as follows:

$$\frac{da}{dN} = C(U\Delta K)^m \tag{14}$$

where U can be represented in the form, $U = C_1 + C_2R + C_3R^2 + --$, where C_1, C_2, C_3, are the constants. The log plot between ΔK and $\frac{da}{dN}$ is sigmoidal in shape and is bounded at the extremes by threshold range, ΔK_{th}, and critical ΔK_c or cyclic fracture toughness of the metal. The above law however doesn't cover crack growth rate in zones A and C i.e. at very low and very high ΔK values. In such zones, continuum mechanics is invalid and the models based on the principles of appropriate micro-fracture based like low cycle fatigue model, as discussed in Section B.2, need to be used.

Decrease in ΔK_{th} results in increased $\frac{da}{dN}$ and vice-versa. Effects of various parameters on ΔK_{th} and $\frac{da}{dN}$ are as follows: i) Increase in grain size without changing the yield strength increases ΔK_{th} and vice-versa ii) Increase in operating temperature reduces ΔK_{th} and vice versa. But in metals that show excessive closure effects the trends may reverse. Enhancement in oxidation rates can cause more closure and may therefore increase ΔK_{th} at

elevated temperature iii) Excessive corrosion results in deposits at crack surfaces that increases ΔK_{th} iv) Inert environments such as vacuum reduce ΔK_{th} by diminishing the effect of oxide induced closure v) Frequency of load cycles does not influence $\frac{da}{dN}$ in ambient and high temperatures but strongly affects it in corrosive environments vi) Increase in stress ratio (+ve value) decreases closure and reduces ΔK_{th} and vice-versa. Reduction in stress ratio (-ve value) increases ΔK_{th} and vice-versa. An overload pulse in the load cycle dips $\frac{da}{dN}$ due to the formation of a larger plastic zone during loading portion that exerts compressive stresses at the crack tip as the zone tries to regain its original shape. An underload pulse is found to increase $\frac{da}{dN}$.

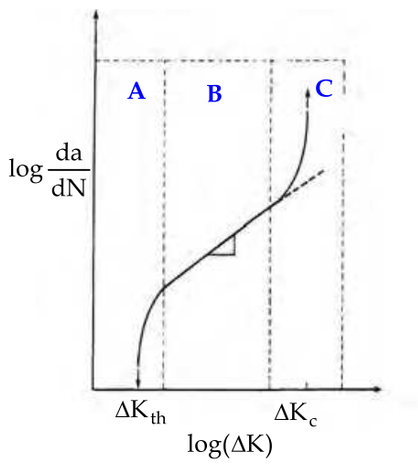

Fig. 18. Long crack growth rate vs applied stress intensity parameter

B.2 *Low cycle regime* [21, pp. 313-318]: Refer Fig. 6. Substituting HRR solution in hysteresis energy, the following expression is obtained on using $r = \delta^* + \rho_c$ and $\theta = 0$ on crack plane:

$$\Delta W^p = \frac{1-n'}{1+n'}\left[\frac{\Delta K^2}{E\psi(n')(\delta^* + \rho_c)}\right] \tag{15}$$

Basquin and Coffin-Manson relationships when coupled yield the following

$$\Delta W^p = 4\left(\frac{1-n'}{1+n'}\right)\sigma_f'\varepsilon_f'(2N_f)^{b+c} \tag{16}$$

The condition for the crack tip to advance through δ^* is obtained from Eq. (15) and Eq. (16) as

$$\frac{\Delta K^2}{E\psi(n')(\delta^* + \rho_c)} = 4\sigma_f'\varepsilon_f'(2N^*)^{-\beta} \tag{17}$$

where $\beta = -(b + c)$. Using crack growth rate, $\frac{da}{dN}$, as $\frac{\delta^*}{N^*}$, one obtains

$$\frac{da}{dN} = \frac{\Delta K^2}{4E\sigma_f' \varepsilon_f' \psi(n')} \frac{(2N^*)^\beta}{N^*} - \frac{\rho_c}{N^*} \tag{18}$$

ρ_c is obtained by using the condition, $\frac{da}{dN} \approx 0$, at $\Delta K = \Delta K_{th}$

$$\rho_c = \frac{\Delta K_{th}^{\ 2}}{4E\sigma_f' \varepsilon_f' \psi(n')} (2N^*)^\beta \tag{19}$$

Eq. (18) and Eq. (19) result in

$$\frac{da}{dN} = 2\delta^* \left[\frac{\Delta K^2 - \Delta K_{th}^{\ 2}}{4E\sigma_f' \varepsilon_f' \delta^* \psi(n')} \right]^{1/\beta} \tag{20}$$

In intermediate Zone B, $\Delta K_{th}^{\ 2}$ can be ignored in comparison with ΔK^2. Therefore, $\frac{da}{dN} = 2\delta^* \left[\frac{\Delta K^2}{4E\sigma_f' \varepsilon_f' \delta^* \psi(n')} \right]^{1/\beta}$, which represents Paris law discussed earlier with coefficients $m = \frac{2}{\beta}$ and $C = 2\left[\frac{1}{4E\sigma_f' \varepsilon_f' \delta^{*(1-\beta)} \psi(n')} \right]^{1/\beta}$.

2.2 Specimen with notch or defect

In such cases, the crack initiates at the edge or corner of a stress concentration site like a notch. The word notch is used here in the generic sense to imply geometric discontinuities of all shapes, e.g. holes, grooves, shoulders (with or without fillets), keyways etc. Crack initiation is easy in notched members vis-à-vis the un-notched ones. Fundamental mechanisms of crack initiation and growth are same as presented in Section 2.1. Some aspects are discussed as follows:

A. Crack initiation life: Underlying principle in dealing with notched members is to relate the crack initiation life at the notch root with that of a smooth uni-axial specimen subjected to an equivalent cyclic load. Local stress and strain at the notch root are first found. Three approaches are then commonly employed i) Local stress or fatigue notch factor approach in which the applied far field or nominal stress range simulated over smooth specimen is K_t times the nominal stress range, $\Delta\sigma_{nom}$, over actual notched component such that $K_t \Delta\sigma_{nom} = (\Delta\sigma_{max} \Delta\varepsilon_{max} E)^{1/2}$ upon using Neuber's law, $K_t^{\ 2} = K_\sigma K_\varepsilon$, where $K_\sigma = \frac{\Delta\sigma_{max}}{\Delta\sigma_{nom}}$ and $K_\varepsilon = \frac{\Delta\varepsilon_{max}}{\Delta\varepsilon_{nom}}$. K_σ, K_ε and K_t are stress concentration, strain concentration and theoretical

stress concentration factor determined from elastic analysis of notched element and $\Delta\sigma_{nom}$, $\Delta\sigma_{max}$, $\Delta\varepsilon_{nom}$ and $\Delta\varepsilon_{max}$ are the cyclic values of nominal stress, maximum stress, nominal strain and maximum strain respectively. K_t in the above has also been replaced by various investigators with fatigue notch factor, K_f, such that $K_f = \frac{\Delta\sigma_{nom}(\text{smooth specimen})}{\Delta\sigma_{nom}(\text{notched specimen})}$ at same fatigue life. Neuber [24] and Peterson [25] have proposed various formulae that relate K_t with K_f ii) Local strain approach in which a smooth specimen is subjected to same strain as that prevailing at the notch root of actual specimen iii) Energy approach which allows to write the following, (Refer Fig. 8 for energy under curve OABDO), $\frac{1}{2}\Delta\sigma_{max}\Delta\varepsilon_{max} = \Delta W = \frac{1}{2}\Delta W^p + \frac{1}{2}\Delta\sigma\Delta\varepsilon$ or $K_t^2\left[\frac{1}{2}\Delta\sigma_{nom}\Delta\varepsilon_{nom}\right] = \frac{1}{2}\Delta W^p + \frac{1}{2}\Delta\sigma\Delta\varepsilon$. On replacing RHS of the equation by general fatigue failure criterion based on single parameter damage representation, one obtains $K_t^2\left[\frac{1}{2}\Delta\sigma_{nom}\Delta\varepsilon_{nom}\right] = \kappa(2N_f)^{\chi} + \Delta W_o$, where ΔW_o is the hysteresis energy at the fatigue limit and is negligible, χ is the slope of plot between $\log\Delta W^p$ and $\log(2N_f)$ and $\log\kappa$ is the intercept ($2N_f = 1$) on the vertical axis. N_f is found accordingly. Initiation is significantly influenced by the radius of curvature of the notch. Fatigue crack nucleates easily at the sharp notch. N_i is small for sharp and high for blunt notches respectively.

B. Crack growth: For small crack of length l, ΔK is equal to $K_t\Delta\sigma_{nom}\sqrt{\pi(a+l)}f(c)$ where a is half notch length that is measured from load axis to the notch tip and f(c) is the configuration factor decided by the dimensions of the crack w.r.t. the body. In an infinite body, f(c) =1. For long crack, the effect of notch is not felt since the crack tip is far away form the notch tip. Therefore, $K_t = 1$ and ΔK equals $\Delta\sigma_{nom}\sqrt{\pi(a+l)}f(c)$.

3. Special cases

3.1 Fatigue under multi - axial load

Many parts in automobiles, aircrafts, pressure vessels etc. operate under multi-axial service load. Consequently, analysis of multi-axial fatigue assumes high importance although it is difficult to precisely define the fatigue behaviour of materials under such loads. When the body is subjected to stress σ_1 under uni-axial load, the state of strain in the body is three-dimensional, i.e. $\varepsilon_2 = e_3 = -\upsilon\varepsilon_1$. There are two stress components acting in the form of normal and shear stress on every plane with only one principal stress, being same as σ_1, acting over the principal plane which is the given plane itself. Multi-axial load is identified with the existence of more than one principal stress and principal plane. In addition, the principal stresses are non-proportional and their magnitude and directions change during the load cycle. Fatigue strength and ductility are found to decrease in multi-axial fatigue. Multi-axial fatigue assessment has been carried out by methods that reduce the complex multi-axial loading to an equivalent uni-axial type. The field of multi-axial fatigue theories

can be classified into five categories i) Empirical formulae resulting after modification of Coffin-Manson Equation ii) Use of stress or strain invariants iii) Use of space averages of stress or strain iv) Critical plane approach and v) Use of accumulated energy. These approaches are elucidated in the succeeding section with the understanding of postulation by Dietmann et al. [26] that in order to determine the resulting fatigue strength of the metal under complex loading , the time dependence of stress wave form, the frequency, the phase difference between stress components and the number of cycles must be considered.

A. *Empirical formulae and modifications of Coffin-Manson equation*: In high cycle fatigue, Lee proposed [27] equivalent stress for a complex load case as, $\sigma_{eq} = \sigma_a\left[1+(b_{fs}C_c/2t_{fs})^{\eta}\right]^{1/\eta}$ where C_c is $2\tau_a/\sigma_a$, $\eta = 2(1+\gamma\sin\phi)$, τ_a is torsional stress amplitude, b_{fs} and t_{fs} are bending and torsional fatigue strength for a given fatigue life respectively, γ is the material constant for consideration of material hardening under out-of-phase loading and ϕ is the phase difference between bending and torsion. σ_{eq} is then used in conventional fatigue life prediction theories stated in Section 1.2.5. Lee and Chiang [28] suggested following equation to consider shear stress that were neglected by other researchers, $\left(\frac{\sigma_a}{b_{fs}}\right)^{b_{fs}(1+\gamma\sin\phi)/t_{fs}} + \left(\frac{\tau_a}{t_{fs}}\right)^{2(1+\gamma\sin\phi)} = \left\{1-\left(\frac{\sigma_m}{\sigma_f'}\right)^{n1}\right\}\left\{1-\left(\frac{\tau_m}{\tau_f'}\right)^{n2}\right\}$ where τ_f' is shear fatigue strength coefficient, τ_m is mean shear stress and n1 and n2 are empirical constants. In low cycle fatigue, Kalluri and Bonacuse [29] suggested the following Coffin-Manson type equation for von-Mises equivalent cyclic strain, $\Delta\varepsilon_{eq} = \left(\frac{\sigma_f'}{E(MF)^{b/c}}\right)(2N_f)^b + \frac{\varepsilon_f'}{MF}(2N_f)^c$ where MF is the multi-axiality factor.

B. *Use of stress or strain invariant*: Sines and Ohgi [30] described fatigue strength with the help of stress invariants in the form, $(J_2')_a^{1/2} \geq A - \alpha_1(J_1)_m - \alpha_2(J_2')_m^n$ where the first stress invariant in terms of principal stresses σ_1, σ_2 and σ_3 is $J_1 = \sigma_1+\sigma_2+\sigma_3$ and $J_2' = \frac{1}{6}\left[(\sigma_1-\sigma_2)^2+(\sigma_2-\sigma_3)^2+(\sigma_3-\sigma_1)^2\right]$, $\alpha_2(J_2')_m^n$ reflects non-linearity effect in case of higher mean stress and n, A, α_1 and α_2 are the material constants. Hashin [31] generalized multi-axial fatigue failure criterion as the function $F(\sigma_{m(ij)}, \sigma_{a(ij)}, \phi_{ij}, 2N_f) = 1$ where ij denotes stress component and ϕ_{ij} is the phase difference between ij stress component and a reference stress component. But the equation is limited to cases of constant load ratio fatigue only.

C. *Use of space averages of stress or strain*: Papadopoulos [32] suggested a generalized failure criterion, $\sqrt{<\tau_m>^2} + \ell\left(\max_t <\sigma_m>\right) \leq \tilde{\lambda}$, where <> indicates average value of the argument acting over critical plane defined by Papadopoulos with ℓ and $\tilde{\lambda}$ being the material constants.

D. *Use of critical plane*: Fatigue analysis upon using the concept of critical plane is very effective because it is based upon the fracture mode or initiation mechanism of cracks. In the critical plane concept, the maximum shear strain or stress plane is first found. Then a parameter is defined as the combination of maximum shear strain or stress and normal strain or stress on the plane to explain multi-axial fatigue behaviour. In high cycle fatigue, McDiarmid [33] proposed equivalent shear stress amplitude as $\tau_a = t_{fs} - \frac{t_{fs} - b_{fs}}{(b_{fs}/2)^{1.5}}\sigma_a^{1.5} - G\sigma_m - 0.081\tau_m$ where G is an empirical constant and stress values are over the maximum shear stress plane. He further suggested [34], $\tau_a = \frac{1}{K_t}\left[t_{fs} - \frac{t_{fs} - b_{fs}}{(b_{fs}/2)^{1.5}}(K_t\sigma_a)^{1.5} - \frac{b_{fs}}{(\sigma_u/2)^2}\sigma_m\right]$ where σ_u is the ultimate tensile strength of metal. In low cycle fatigue, Brown and Miller [35] derived the relation, $\gamma_{max,pl} + \varepsilon_{n,pl} + \sigma_{no}/E = \gamma_f'(2N_f)^v$, where maximum plastic shear strain, $\gamma_{max,pl}$, and normal plastic strain, $\varepsilon_{n,pl}$, are the values of Brown and Millers parameters, σ_{no} is the component of mean stress on γ_{max} plane and v and γ_f' are shear fatigue ductility exponent and coefficient respectively. Socie [36] suggested the following for shear cracking mode, $\gamma_{max} + \varepsilon_n + \sigma_{no}/E = \gamma_f'(2N_f)^v + \frac{\tau_f'}{G}(2N_f)^w$, where w is the shear fatigue strength exponent and for tensile cracking mode, $\sigma_1^{max}\Delta\varepsilon_1/2 = \sigma_f'\varepsilon_f'(2N_f)^{b+c} + (\sigma_f')^2(2N_f)^{2b}/E$. Fatemi and Socie [37] modified Brown and Millers equation as follows: $\gamma_{max}\left(1 + n\frac{\sigma_n^{max}}{\sigma_y}\right) = (1+\nu_e)\frac{\sigma_f'}{E}(2N_f)^b + \frac{n}{2}(1+\nu_e)\frac{(\sigma_f')^2}{E\sigma_y}(2N_f)^{2b} + (1+\nu_p)\varepsilon_f'(2N_f)^c + \frac{n}{2}(1+\nu_p)\frac{\varepsilon_f'\sigma_f'}{\sigma_y}(2N_f)^{b+c}$ where n is an empirical constant, ν_e and ν_p are poisson's ratio in elastic and plastic regions respectively.

E. *Use of energy concepts*: All aforementioned stress or strain based criteria don't consider multi-axial stress-strain response of the material. The fatigue process is generally believed to involve cyclic plastic deformations which are dependent on stress-strain path. Thus, stress or strain based criteria alone cannot reflect the path dependence on fatigue process sufficiently. After initial work by Garud [38], Ellyin and Golos [39] proposed that durability of components should be characterized with the quantity of energy which a material can contain and suggested total strain energy density, ΔW_t, as sum of elastic and plastic components as follows: $\Delta W_t = \Delta W_e + \Delta W_p$ where $\Delta W_e = \frac{1+\nu}{3E}(\bar{\sigma}^{max})^2 + \frac{1-2\nu}{6E}(\sigma_{kk}^{max})^2$, $\Delta W_p = \frac{2(1-n')(2\sigma_f')^{-1/n'}}{1+n'}(\Delta\bar{\sigma})^{\frac{1+n'}{n'}}$, $\bar{\sigma}$ being the von-Mises equivalent stress. However, these equations do not include the effect of strain ratio. Besides, they don't explain the additional cyclic hardening or softening of material due to interaction between loadings under out of phase multi-axial loading. Such problems were overcome by Ellyin et al. [40] who performed in-phase and out of phase multi-axial fatigue tests by using multi-axial constraint factor (MCF) to supplement the results of Ellyin and Golos.

3.2 Fatigue under aqueous and corrosive environments

Naval structures consistently work under such environments. There are various factors that influence environment assisted fracture of a metal namely its alloy chemistry, heat treatment, atmospheric humidity and temperature, salt concentration in air and work hardening of metal. It is generally agreed that presence of aggressive aqueous environment drastically reduces the fatigue life of metal. Initiation or nucleation life of fatigue crack in a polished specimen may drop to just 10% of total fatigue life in corrosive environment. Exposure to corrosive environment probably has the same effect on fatigue life as machining of sharp notch into the surface. Corrosive environment facilitates development of geometric discontinuities on the surface. These discontinuities or stress risers then become the potential sites for origination of fatigue cracks upon cyclic loading. The mechanisms of initiation and growth of crack in corrosive environment [41] are discussed below (It is important to mention here that no single mechanism can fully explain crack initiation or crack propagation behaviour of metals in corrosive environment):

A. *Crack initiation*: Several mechanisms have been proposed. They are i) Surface film rupture - In this method, nucleation is caused by mechanical damage to the protective surface film. Most metals have a thin oxide layer on their surface. This thin layer, being passive in metals, protects the metal from atmospheric moisture. In addition, both anodic and cathodic corrosion reaction sites exist on the surface of metal when exposed to aqueous solution leading to formation of a protective layer. But when the part is subjected to mechanical stressing, the film is broken resulting in exposure of fresh metal to the environment which may then act as an anodic or cathodic reaction site causing accumulation of foreign corrosive particles which act as discontinuities and potential fatigue sites ii) Pitting – Corrosion pits may be formed on and beneath the surface that assist in nucleation of fatigue cracks. High dissolution rate in the pit could unblock piled up dislocations and allow slip to occur. iii) Strain effects – Strain enhanced dissolution of emerging slip bands promotes nucleation iv) Surface adsorption – Surface energy of metal is lowered by adsorption of specific species from the environment. Reduction in surface energy enhances plasticity and early crack initiation.

B. *Crack propagation*: Two main mechanisms assist in crack growth. They are i) Anodic dissolution - When the metal is exposed to aqueous solution, it loses metallic ions close to the crack tip. The loss of ions leaves extra electrons on the surface thus making the crack tip behave as an anode of the electrolytic cell. Anodic dissolution causes growth of the crack tip within a grain till it reaches the grain boundary thus exposing the grain boundary for hydrogen embrittlement ii) Hydrogen embrittlement - Owing to tensile stresses in the vicinity of crack tip during cyclic load, the hydrogen atoms, being small in size, diffuse into grain boundaries, voids, inclusions and highly strained slip bands. The diffusion is usually slow but makes the material in the vicinity of crack tip brittle and the crack is no longer able to withstand applied ΔK. Consequently, the crack grows up to the point only where the effect of hydrogen embrittlement is diminished and the whole process then repeats itself. There are two ways in which crack grows in corrosive environment. Refer Fig. 19. i) True corrosion fatigue (TCF) in which crack growth rates are enhanced by the presence of aggressive environment through a synergistic action of corrosion and cyclic loading. TCF is characterized by environment induced change on the values for conventional Paris constants C and m. TCF is observed till ΔK is less than ΔK_{iscc} where ΔK_{iscc} represents

threshold stress corrosion cracking intensity range which is material property under given environment ii) Stress corrosion fatigue (SCF) starts when ΔK exceeds ΔK_{iscc}. SCF describes static load stress concentration under fatigue conditions. Either TCF or SCF can be induced by changing the frequency and stress ratio. The kinetic processes that take place during crack growth are summarized as i) Supply of reactants and removal of products from the crack tip region ii) Reactions at the crack tip surface iii) Diffusion of atoms ahead of the crack tip iv) Partitioning of ions at various micro-structural sites v) Rupture of protective film during cyclic loading vi) Development of freshly fractured surfaces by fatigue processes and vii) Build up of corrosion products that influence crack closure and effective ΔK.

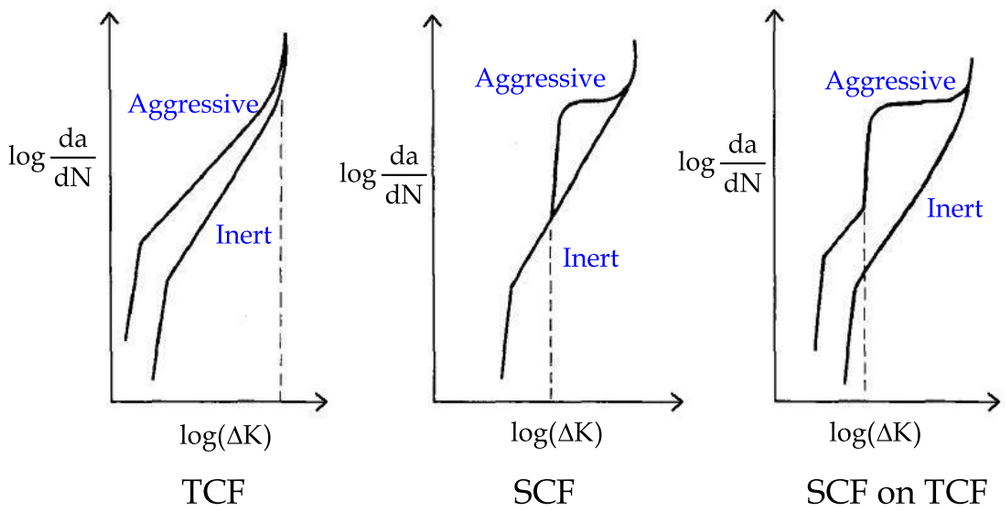

Fig. 19. Types of corrosion fatigue

B.1 *Crack propagation models*: The following models are proposed i) Process superposition model in which general form of crack growth is written by summing crack growth rates for pure mechanical fatigue and corrosion fatigue as follows: $\frac{da}{dN}=\left(\frac{da}{dN}\right)_f(1-\varphi)+\left(\frac{da}{dN}\right)_{scc}+\left(\frac{da}{dN}\right)_c\varphi$ where $\left(\frac{da}{dN}\right)_f$ represents contribution of pure mechanical fatigue (in an inert environment and independent of frequency), $\left(\frac{da}{dN}\right)_{scc}$ is contribution by corrosion at test levels above ΔK_{iscc}, $\left(\frac{da}{dN}\right)_c$ is a cycle dependant contribution that represents synergistic interaction between mechanical fatigue and stress corrosion cracking and φ stands for fractional area of crack undergoing pure corrosion fatigue ii) Process competition model in which the crack growth rate equation is written in style of Paris equation as, $C_1(\Delta K)^{m1}=C(\Delta K+d\Delta K)^m$, where constants C_1 and m_1 are constants of fatigue in corrosive environment and $d\Delta K$ represents corrosion fatigue contribution iii) Process interaction model which accounts for the fact that corrosive products at crack tip may cause closure thereby reducing crack growth rate. But the overall

effect of such products is to enhance the crack growth rate. Likewise, the effect of frequency is included in this model. The crack growth rate is written as $\frac{da}{dN} = C(\Delta K)_{eff}^{m} + \int_{0}^{1/f} A\varsigma\Delta K_{eff}{}^{\wp}dt$ where $(\Delta K)_{eff}$ takes into account the effects of closure, blunting and branching, the term ς includes the influence of load cycle on stress corrosion rate, f being the frequency and A and $\wp$ the constants that are experimentally obtained.

3.3 Fatigue under high temperature

Gas turbines, aircraft engines, nuclear reactors etc. operate in such an environment. The metal is said to be operating in high temperature environment when the temperature level is ≥ 0.5 times the melting point of the metal. New effects like atmospheric oxidation and creep supplement fatigue at high temperature. Metal alloys are usually designed and developed to have good creep strength at high temperatures under static loads. Because alloys with good resistance to creep generally exhibit acceptable fatigue strength up to a certain limiting temperature. But beyond that, the rate of damage in metals increases due to creep dominance coupled with fatigue resistance reduction resulting in shorter lives. The fundamental crack initiation and growth mechanisms explained earlier in Section 2 hold good at high temperature except the location of crack initiation site, subsequent path of crack propagation, crack growth rate and the quantum of damage induced with time. Since creep forms an important aspect at high temperature, corresponding fatigue models are time based. Some aspects are presented as follows:

A. Crack initiation: Most metals when subjected to cyclic load under high temperature show damage in the form of grain-boundary voids and wedge cracks, as shown in Fig. 10, because of high energy levels at the grain boundary. The latter requires grain boundary sliding which results in geometric incompatibility at 'triple points' leading to the stress concentration or crack nucleation site. Therefore, a cavity nucleates whose growth is sustained by stress assisted diffusion or grain boundary sliding or the combination of the two. Rather high tensile stresses are required to maintain the cavity. Other factors such as migration of fatigue generated vacancies, segregation of impurities and diffusion and development of internal gas pressure also contribute to the stability of the cavity.

B. Crack growth: Nucleated cavities grow along grain boundaries that are generally perpendicular to the maximum principal stress direction as shown in Fig. 20. Crack closure is more at high temperature that influences crack growth rates. Therefore, ΔK_{eff} is introduced and Paris law is modified to the form, $\frac{da}{dN} = C\left(\frac{\Delta K_{eff}}{K_o(R)}\right)^{m(R)}$, where parameters K_o and m depend upon the stress ratio, R.

C. *Life prediction methods*: Life prediction in high temperature fatigue can be grouped into five categories namely i) Linear summation of time and cycle [42,43] ii) Modifications of low-temperature fatigue relationships [44] iii) Ductility exhaustion [45] iv) Strain range partitioning [46] and v) Continuous damage parameter [47-49]. For example, the model

due to i) is written as $\frac{N}{N_f}+\int\frac{dt}{t_R}=1$ where N is actual life under creep fatigue, N_f is fatigue life without creep and t_R is the creep rupture time.

The damage can be assumed to comprise two functions, namely rate independent (mechanical fatigue), Ω_f , and rate dependant (creep damage) component, Ω_c and is written as $D = D(\Omega_f, \Omega_c)$. The rate of damage accumulation per cycle is then represented as $\frac{dD}{dN}=\frac{\partial D}{\partial \Omega_f}\frac{\partial \Omega_f}{dN}+\frac{\partial D}{\partial \Omega_c}\frac{\partial \Omega_c}{dN}$.

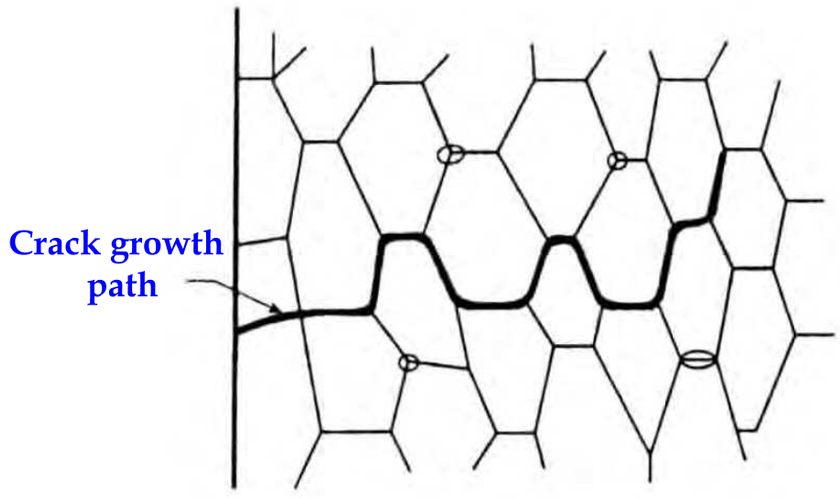

Fig. 20. Crack growth along grain boundaries at high temperature

3.4 Giga cycle fatigue

Giga or ultra high cycle fatigue has assumed importance in the design of high speed components in modern machines, the desired life of some of them ranging from 10^8 to 10^{10} cycles. This requirement is applicable to sectors like aircraft (gas turbine disks-10^{10} cycles), railway (high speed train-10^9 cycles) and automobile (car engine-10^8 cycles). Although large amount of fatigue data has been published in the form of S–N curves, the data are mostly limited to fatigue lives of 10^7 cycles. Time and cost constraints rule out the use of conventional fatigue tests for more than 10^7 cycles. Conventional test conducted at frequency of 20 Hz may require several years for generating 10^{10} cycles to test one specimen. During initial development by Wohler, gigacycle tests didn't assume importance because many industrial applications during that time, such as steam engines etc. , had a small fatigue life in comparison with modern machines. Therefore, gigacycle fatigue is more appropriate for modern technologies. The major challenge in measuring fatigue strength in gigacycle regime lies in generating very high frequencies that save time and also do not produce erroneous results by affecting basic mechanisms of crack initiation and propagation since the structure in normal operation shall have to perform under conventional frequency of smaller magnitudes.

Since the effect of frequency on fatigue life of metal is negligible in normal ambient conditions, piezoelectric based, ultrasonic fatigue machines [50] are used to generate high frequencies of the order of 20 kHz. They are reported to be reliable and capable of producing 10^{10} cycles in less than a week. But, as expected, lot of heat is generated during such a test. The temperature of the specimen is therefore continuously monitored by thermo couples for regular cooling. In some steels, the gap between fatigue strengths corresponding to 10^7 and 10^{10} cycles can reach up to 200 MPa. Therefore gigacycle machines are operated at lower stress value that should be correctly known for failure free performance of such machines.

4. Acknowledgement

Support received from the School of Mechanical and Building Sciences, VIT, Vellore during the course of this work is gratefully acknowledged.

5. References

[1] Wohler, A. (1860). Versuche uber die Festigkeit der Eisenbahnwagenachsen, *Zeitschrift fur Bauwesen*,10; English summary (1867), *Engineering*, Vol.4, pp.160-161.

[2] Campbell Glen, S. (1981). A note on fatal aircraft accidents involving metal fatigue, *International Journal of Fatigue*, Vol.3, pp. 181-185.

[3] Callister William, D. (2003). Failure, In: *Materials Science and Engineering: An Introduction*, pp. 215-217, John Wiley and sons, Inc.

[4] Basquin, O.H. (1910). The exponential law of endurance tests, *Proceedings of ASTM*, Vol. 10(II), pp. 625-630.

[5] Coffin Jr., L.F. (1954). A study of the effects of cyclic thermal stresses on a ductile metal, *Trans. ASME*, Vol. 76, pp. 931-950.

[6] Manson, S.S. (1954). Behaviour of materials under conditions of thermal stress, *NACA TN-2933*, National Advisory Committee for Aeronautics.

[7] Miner, M.A. (1945). Cumulative damage in fatigue, *Journal of Applied Mechanics*, Vol. 67, pp. A159-A164.

[8] Palmgren, A. (1924). Die Lebensdauer von Kugellagern, *Verfahrenstechinik, Berlin*, Vol. 68, pp. 339-341.

[9] Richart, F.E. and Newmark, N.M. (1948). An hypothesis for the determination of cumulative damage in fatigue, *Proceedings of ASTM*, Vol. 48, pp. 767-800.

[10] Marco, S.M. and Starkey, W.L. (1954). A concept of fatigue damage, *Trans. ASME,* Vol. 76, pp. 627-632.

[11] Kommers, J.B. (1945). The effect of overstress in fatigue on the endurance limit of steel, *Proceedings of ASTM*, Vol. 45, pp. 532-541.

[12] Bennett, J.A. (1946). A study of the damaging effect of fatigue stressing on X4130 steel, *Proceedings of ASTM*, Vol. 46, pp. 693-714.

[13] Corten, H.T. and Dolon, T.J. (1956). Cumulative fatigue damage, *Proceedings of the International Conference on Fatigue of Metals,* Institution of Mechanical Engineering and American Society of Mechanical Engineers, pp. 235-246.

[14] Freudenthal, A.M. and Heller, R.A. (1959). On stress interaction in fatigue and a cumulative damage rule, *Journal of the Aerospace Sciences,* Vol. 26, pp. 431-442.
[15] Langer, B.F. (1937). Fatigue failure from stress cycles of varying amplitude, *ASME Journal of Applied Mechanics*, Vol. 59, pp. A160-A162.
[16] Grover, H.J. (1960). An observation concerning the cycle ratio in cumulative damage, *Symposium on Fatigue of Aircraft Structures, ASTM STP 274,* ASTM, Philadelphia, PA, pp.120-124.
[17] Manson, S.S. (1966). Interfaces between fatigue, creep and fracture, *International Journal of Fracture*, Vol. 2, pp. 328-363.
[18] Ellyin, F. (1985). A strategy for periodic inspection based on defect growth, *Theoretical and Applied Fracture Mechanics*, Vol. 4, pp. 83-96.
[19] Taylor, D. (1989). Theories and mechanisms, In: *Fatigue Thresholds*, p. 13. Butterworths.
[20] Morrow, J.D. (1965). Cyclic plastic strain energy and fatigue of metals, In: *Internal Friction, Damping and Cyclic Plasticity, ASTM STP 378,* Philadelphia, PA, pp. 45-84.
[21] Ellyin, F. (1997). Phenomenological approach to fatigue life prediction under uniaxial loading, In: *Fatigue Damage, Crack Growth and Life Prediction*, pp. 88-90, Chapman and Hall.
[22] Laird, C. and Smith, G.C. (1963). Initial stages of damage in high stress fatigue in some pure metals, *Phil. Mag*., Vol. 8, pp. 1945-1963.
[23] Paris, P.C., Gomez, M.P. and Anderson, W.E. (1961). A rational analytic theory of fatigue, *The Trend in Engineering*, Vol. 13, pp. 9-14, University of Washington, Seatle (WA).
[24] Neuber, H. (1958). Theory of notch stress, *Kerbspannungslehre*, Springer, Berlin.
[25] Peterson, R.E. (1974). *Stress Concentration Factors*, John Wiley, New York.
[26] Dietmann, H., Bhongbhidhat, T. and Schmid, A. (1991). Multi-axial fatigue behaviour of steels under in-phase and out-of-phase loading including different waveforms and frequencies, In: *Fatigue under bi-axial and multi-axial loading*, p. 449, ESIS10, Mechanical Engineering Publications, London.
[27] Lee, S.B. (1980). Evaluation of theories on multi-axial fatigue with discriminating specimens, Ph.D. Thesis, Stanford University, Stanford.
[28] Lee, Y.L. and Chiang, Y.J. (1991). Fatigue predictions for components under bi-axial reversed loading, *Journal of Testing and Evaluation*, Vol. 19, p. 359.
[29] Kalluri, S. and Bonacuse, P.J. (1993). In-phase and out-of-phase axial-torsional fatigue behaviour of Haynes 188 superalloy at 760 deg. C., In: *Advances in multi-axial fatigue,* ASTM STP 1191, p.133.
[30] Sines, G. and Ohgi, G. (1981). Fatigue criteria under combined stresses or strains, *Journal of Engineering Materials and Technology,* Trans. ASME, Vol. 103, p.82.
[31] Hashin, Z. (1981). Fatigue failure criteria for combined cyclic stress, *International Journal of Fracture,* Vol. 17, p. 101.
[32] Papadopoulos, I.V. (1994). A new criterion of fatigue strength for out-of-phase bending and torsion of hard metals, *International Journal of Fatigue,* Vol. 16, p. 377.

[33] McDiarmid, D.L. (1985). The effects of mean stress and stress concentration on fatigue under combined bending and twisting, *Fatigue and Fracture of Engineering Materials and Structures*, Vol. 8, p.1.

[34] McDiarmid, D.L. (1987). Fatigue under out-of-phase bending and torsion, *Fatigue and Fracture of Engineering Materials and Structures*, Vol.9, p. 457.

[35] Brown, M.W. and Miller, K.J. (1982). Two decades of progress in the assessment of multi-axial low cycle fatigue life, In: *Low cycle fatigue and life prediction*, ASTM STP 770, p. 482.

[36] Socie, D. (1987). Multi-axial fatigue damage models, *Journal of Engineering Materials and Technology,* Trans. ASME, Vol. 109, p. 293.

[37] Fatemi, A. and Socie, D.F. (1988). A critical plane approach to multi-axial fatigue damage including out-of-phase loading, *Fatigue and Fracture of Engineering Materials and Structures*, Vol. 11, p. 149.

[38] Garud, Y.S. (1979). A new approach to the evaluation of fatigue under multi-axial loading, *Proceedings of Symposium on Methods for Predicting Material Life in Fatigue,* p. 247, ASME.

[39] Ellyin, F. and Golos, K. (1988). Multi-axial fatigue damage criterion, *Journal of Engineering Materials and Technology,* Trans. ASME, Vol. 110, p. 63.

[40] Ellyin, F., Golos, K. and Xia Z. (1991). In-phase and out-of-phase multi-axial fatigue, *Journal of Engineering Materials and Technology,* Trans. ASME, Vol. 113, p. 112.

[41] Sudarshan, T.S., Srivatsan, T.S. and Harvey II, D.P. (1990). Fatigue processes in metals-Role of aqueous environments, *Engineering Fracture Mechanics*, Vol. 36, pp. 827-852.

[42] Robinson, E.L. (1952). Effect of temperature variation on the long time rupture strength of steels, *Trans. ASME*, Vol. 74, pp. 777-781.

[43] Taira, S. (1962). Lifetime of structures subjected to varying load and temperature, In: *Creep in structures*, Academic Press, pp. 96-124.

[44] Coffin, L.F. (1973). Fatigue at high temperatures, In: *Fatigue at high temperatures*, ASTM STP 520, pp. 5-43.

[45] Polhemus, J.F., Spaeth, C.E. and Vogel, W.H. (1973). Ductility exhaustion model for prediction of thermal fatigue and creep interaction, In: *Fatigue at elevated temperatures*, ASTM STP 520, pp. 625-636

[46] Manson, S.S., Halford, G.R., and Hirschberg, M.H. (1971). Creep-fatigue analysis by strain range partioning, In: *Design for elevated temperature environment*, ASME, pp. 12-24.

[47] Kachanov, L.M. (1999). Rupture time under creep conditions, *International journal of fracture*, Vol. 97, pp. 1-4.

[48] Majumdar, S. and Maiya, P.S. (1980). A mechanistic model for time-dependent fatigue, *Journal of Engineering Materials and Technology*, Trans. ASME, Vol. 102, pp. 159-167.

[49] Majumdar, S. (1964). Relationships of creep, creep-fatigue and cavitation damage in Type 304 austenitic stainless steels, *Journal of Engineering Materials and Technology*, Trans. ASME, Vol. 111, pp. 123-131.

[50] Marines, I., Bin, X. and Bathias, C. (2003). An understanding of very high cycle fatigue of metals, *International Journal of Fatigue*, Vol. 25, pp. 1101-1107.

IntechOpen

IntechOpen

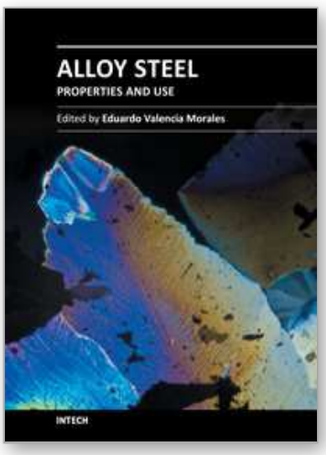

Alloy Steel - Properties and Use

Edited by Dr. Eduardo Valencia Morales

ISBN 978-953-307-484-9
Hard cover, 270 pages
Publisher InTech
Published online 22, December, 2011
Published in print edition December, 2011

The sections in this book are devoted to new approaches and usages of stainless steels, the influence of the environments on the behavior of certain classes of steels, new structural concepts to understand some fatigue processes, new insight on strengthening mechanisms, and toughness in microalloyed steels. The kinetics during tempering in low-alloy steels is also discussed through a new set-up that uses a modified Avrami formalism.

How to reference

In order to correctly reference this scholarly work, feel free to copy and paste the following:

S. Bhat and R. Patibandla (2011). Metal Fatigue and Basic Theoretical Models: A Review, Alloy Steel - Properties and Use, Dr. Eduardo Valencia Morales (Ed.), ISBN: 978-953-307-484-9, InTech, Available from: http://www.intechopen.com/books/alloy-steel-properties-and-use/metal-fatigue-and-basic-theoretical-models-a-review

INTECH
open science | open minds

InTech Europe
University Campus STeP Ri
Slavka Krautzeka 83/A
51000 Rijeka, Croatia
Phone: +385 (51) 770 447
Fax: +385 (51) 686 166
www.intechopen.com

InTech China
Unit 405, Office Block, Hotel Equatorial Shanghai
No.65, Yan An Road (West), Shanghai, 200040, China
中国上海市延安西路65号上海国际贵都大饭店办公楼405单元
Phone: +86-21-62489820
Fax: +86-21-62489821

© 2011 The Author(s). Licensee IntechOpen. This is an open access article distributed under the terms of the Creative Commons Attribution 3.0 License, which permits unrestricted use, distribution, and reproduction in any medium, provided the original work is properly cited.

IntechOpen

IntechOpen